

## Supporting Information: *In-situ* generation of fullerene from a poly(fullerene)

Hugo Santos Silva,<sup>1,2</sup> Hasina H. Ramanitra,<sup>1,2</sup> Bruna A. Bregadiolli,<sup>1,3</sup> Aurélien Tournebize,<sup>2</sup> Didier Bégué,<sup>1</sup> Simon Dowland,<sup>4</sup> Christine Lartigau-Dagron,<sup>1</sup> Carlos F. O. Graeff,<sup>3</sup> Andreas Distler,<sup>4</sup> Heiko Peisert,<sup>2</sup> Thomas Chassé,<sup>2</sup> Roger C. Hiorns<sup>1\*</sup>

<sup>1</sup> CNRS/Univ Pau & Pays Adour, Institut des Science Analytiques et Physico-Chimie pour l'Environnement et les Matériaux, Pau, France

<sup>2</sup> Institute for Physical and Theoretical Chemistry, Eberhard Karls Universität Tübingen, Auf der Morgenstelle 18, 72076 Tübingen, Germany.

<sup>3</sup> Departamento de Física – FC – UNESP, Av. Luiz Edmundo Carrijo Coube, 14-01, 17033-360 Bauru, Brazil.

<sup>4</sup> OPVIUS OPV GmbH, Landgrabenstraße 94, 90443 Nürnberg, Germany.

\*roger.hiorns@univ-pau.fr

### Contents

Equipment

Experimental

- Figure S1. OPV properties of cells using HSS-12 as acceptor materials.
- Figure S2. OPV properties of cells using HSS-12 as an additive
- Figure S3. Gaussian fits of the UV-visible spectrum of a thin solid film of HSS-12.
- Figure S4. Overview XPS spectrum of HSS-12 deposited on to ITO/glass.
- Figure S5. Carbon 1s XPS peaks from HSS-12 thin films on ITO/glass following annealing.
- Figure S6. Evolution of surface roughness of P3HT:PCBM and P3HT:PCBM:HSS-12 with time.
- Figure S7. Overview XPS spectra for P3HT:PCBM and P3HT:PCBM:HSS-12 blends at  $t = 0$ .
- Table S1. XPS indicated relative elementary concentrations with annealing in thin-film blends.
- Figure S8. C1s core level spectra of HSS-12 as a function of the irradiation time.
- Figure S9. 3D AFM reconstructions of (a) P3HT:PCBM and (b) P3HT:PCBM:HSS-12 nanomorphologies illuminated under AM1.5 conditions and nitrogen atmosphere for 120 h.
- Table S2. XPS indicated relative atomic concentrations in thin-film blends before and after treatment with light under AM1.5 conditions and N<sub>2</sub>.
- Figure S10. Evolution of UV-visible spectra under AM1.5 conditions and synthetic air.
- Figure S11. Evolution of UV-visible spectra under photo-oxidation conditions with respect to the pristine sample.
- Figure S12. Carbon 1s XPS peak for HSS-12 polymer (thin film on ITO/glass substrate) submitted under irradiation times under synthetic air atmosphere.
- Figure S13. Oxygen 1s XPS spectra for HSS-12 polymer (thin film on ITO/glass substrate) submitted under irradiation times under synthetic air atmosphere.
- Figure S14. Evolution in time of HSS-12 FTIR spectra during photo-oxidation.
- Figure S15. Evolution with photo-oxidation of the UV-visible spectra of: (a) P3HT:PCBM; and (b) P3HT:PCBM:HSS-12.
- Figure S16. Evolution with time of the UV-visible spectra of P3HT:PCBM and P3HT:PCBM:HSS-12 undergoing photo-oxidation.
- Figure S17. Bond-dissociation reaction coordinate scan for the ATRAP proposed model material calculated by different level of theories, under optimization or single-point energy evaluations.
- Figure S18. Modified ATRAP structures used to study the influence of the -CH<sub>2</sub>- link on stabilities.
- Figure S19. Three possible products of degradation resulting from the formation *p*-quinodimethane during the thermal treatment of PFBMBs.
- Figure S20. <sup>1</sup>H-NMR spectra of HSS-12 in *d*<sub>8</sub>-toluene solution heated to 100 °C for 16 h in a nitrogen-sealed glass tube.
- Figure S21. <sup>1</sup>H-NMR spectra of HSS-12 *d*<sub>8</sub>-toluene solution heated to 100 °C for 16 h - 3.5-5.0 ppm region.
- Figure S22. <sup>1</sup>H-NMR spectra of HSS-12 *d*<sub>8</sub>-toluene solution heated to 100 °C for 16 h - zoom in the aromatic regions.

References

## **Equipment**

### ***XPS***

Photoemission measurements were performed at an ultra high vacuum (UHV) system equipped with a Phoibos 150 hemispherical analyser (SPECS), a monochromatic AlK $\alpha$  source and a high-flux He discharge lamp (UVS 300, SPECS). Peak fitting of XPS spectra was carried out using the program Unifit.<sup>1</sup> For the calculation of the atomic composition, atomic cross sections for photoionization from Yeh and Lindau<sup>2</sup> were used.

### ***AFM***

A Nanoscope IIIa atomic force microscope (AFM) from Veeco Instruments was used for surface topography measurements. Images were obtained using “tapping” mode.

### **Preparation of OPV Devices**

The standard architecture was based around ITO/ZnO/P3HT:PCBM/PEDOT:PSS/Ag. ITO substrates were cleaned by sonication in acetone followed by isopropanol. A ZnO nanoparticle suspension (5 wt% in ethanol) was then coated onto the clean substrates and annealed at 140 °C in air. In cases where a PFBMB interlayer was used this was coated directly onto the ZnO from a xylene solution. The active layer was coated from a blend solution containing various ratios of P3HT : PCBM : PFBMB in 27 mg ml<sup>-1</sup> o-xylene (+5% 1-methylnaphthalene) solutions. A layer of PEDOT:PSS was coated from a stock solution diluted with 3 parts isopropanol and subsequent annealing in nitrogen at 140 °C for 5 min. All aforementioned depositions were carried out with a doctor blade. The devices were completed by thermal evaporation of silver under high vacuum to produce cells with 27 mm<sup>2</sup> active area. The current voltage characteristics were measured under N<sub>2</sub> using a Keithley 2400 source meter and a Xenon arc lamp with an intensity of approximately 100 mW cm<sup>-2</sup>. Where single-material layers were required for other characterisations, such as XPS, the same methodology was used.

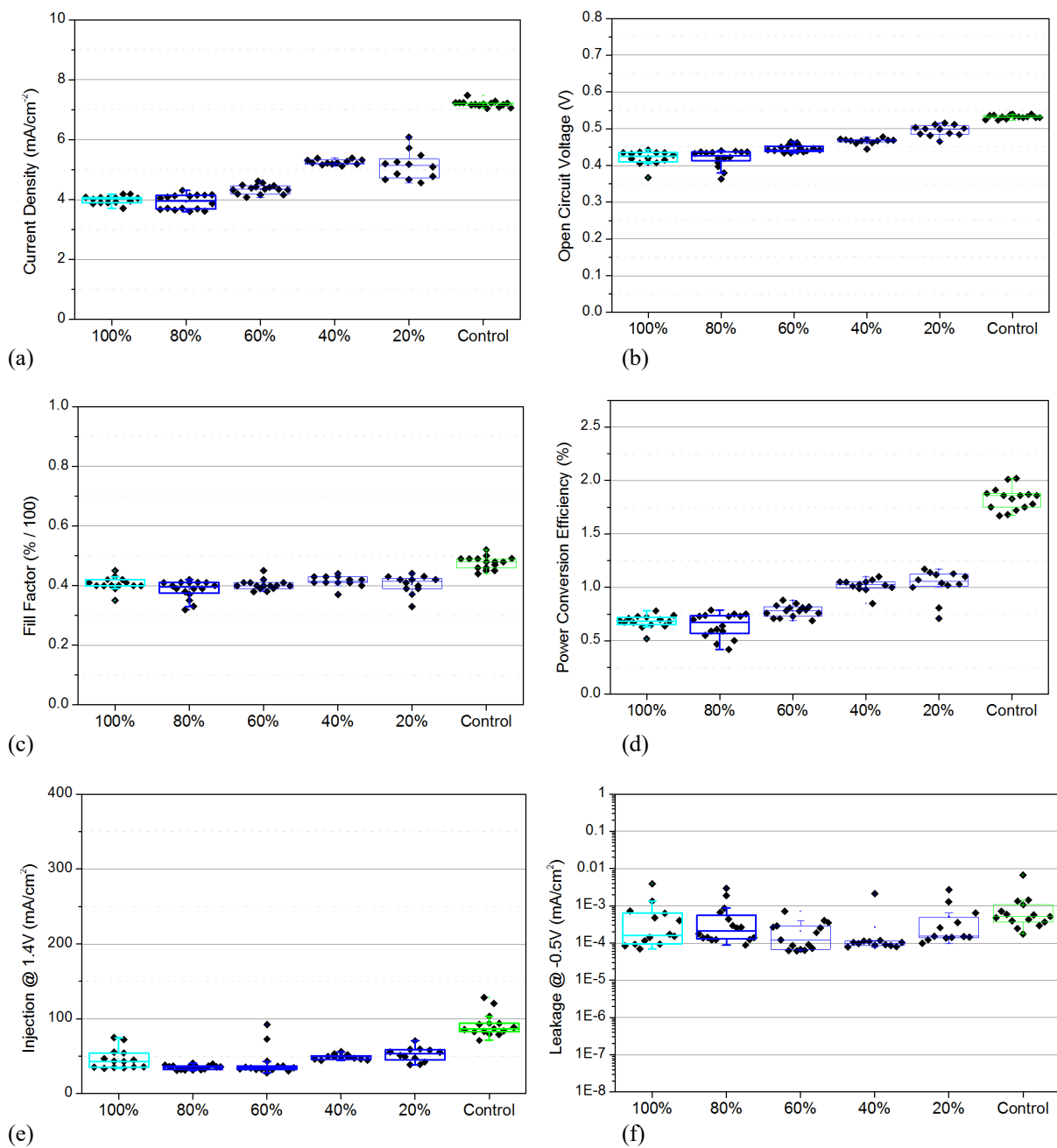


**Figure S1.** OPV properties of cells using HSS-12 as acceptor material with different loads of HSS-12 compared to PCBM. The x-axis indicates the load of HSS-12. (a)  $J_{sc}$ s; (b)  $V_{oc}$ s; (c) FFs; (d) PCEs; (e) injection currents; and (f) leakage currents.

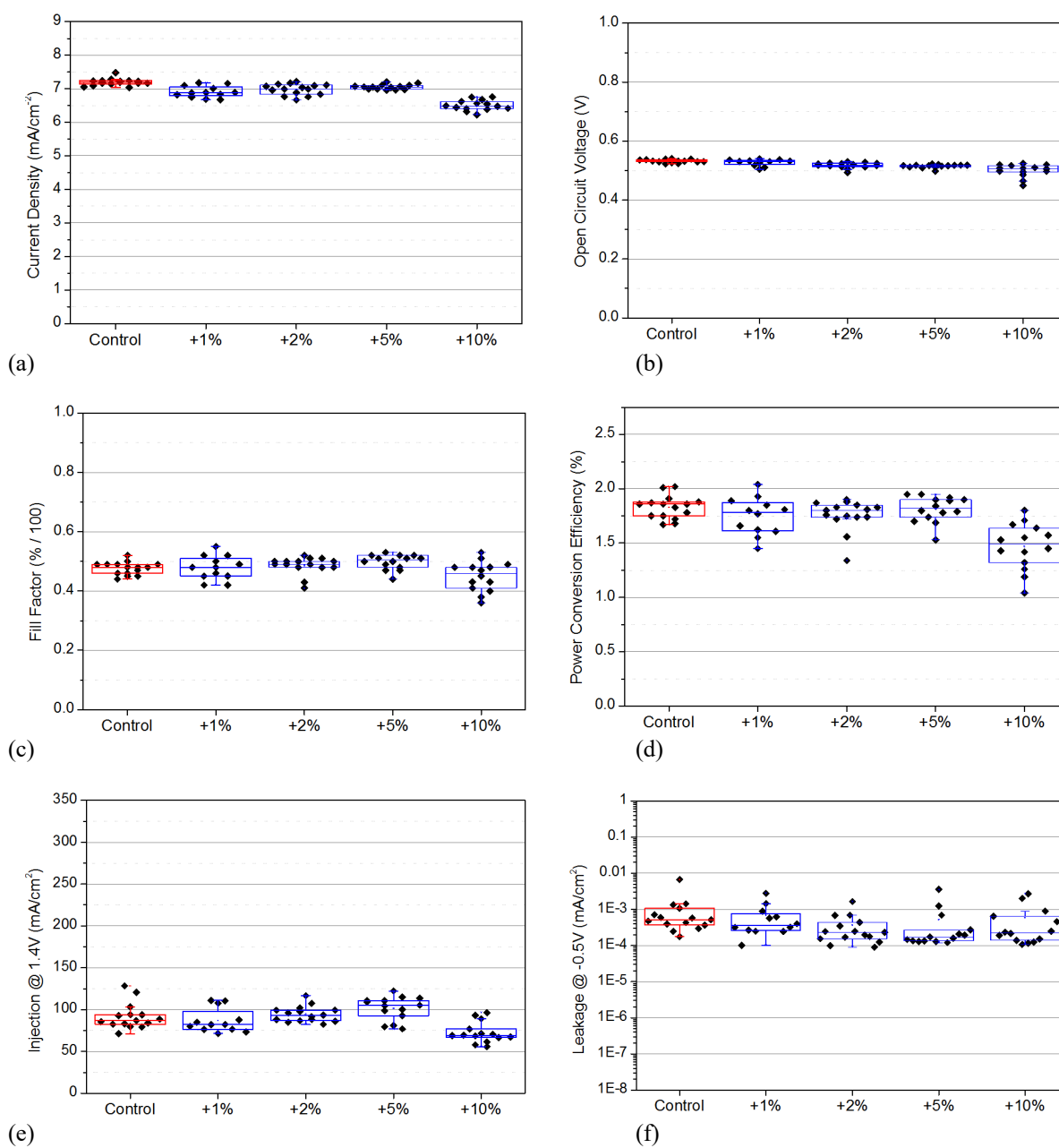


**Figure S2.** OPV properties of cells using HSS-12 as an additive to the blend with different loads of HSS-12 compared to PCBM. The x-axis indicates the load of HSS-12. (a)  $J_{\text{sc}}$ ; (b)  $V_{\text{oc}}$ ; (c)  $FF$ s; (d) PCEs; (e) injection currents; and (f) leakage currents.

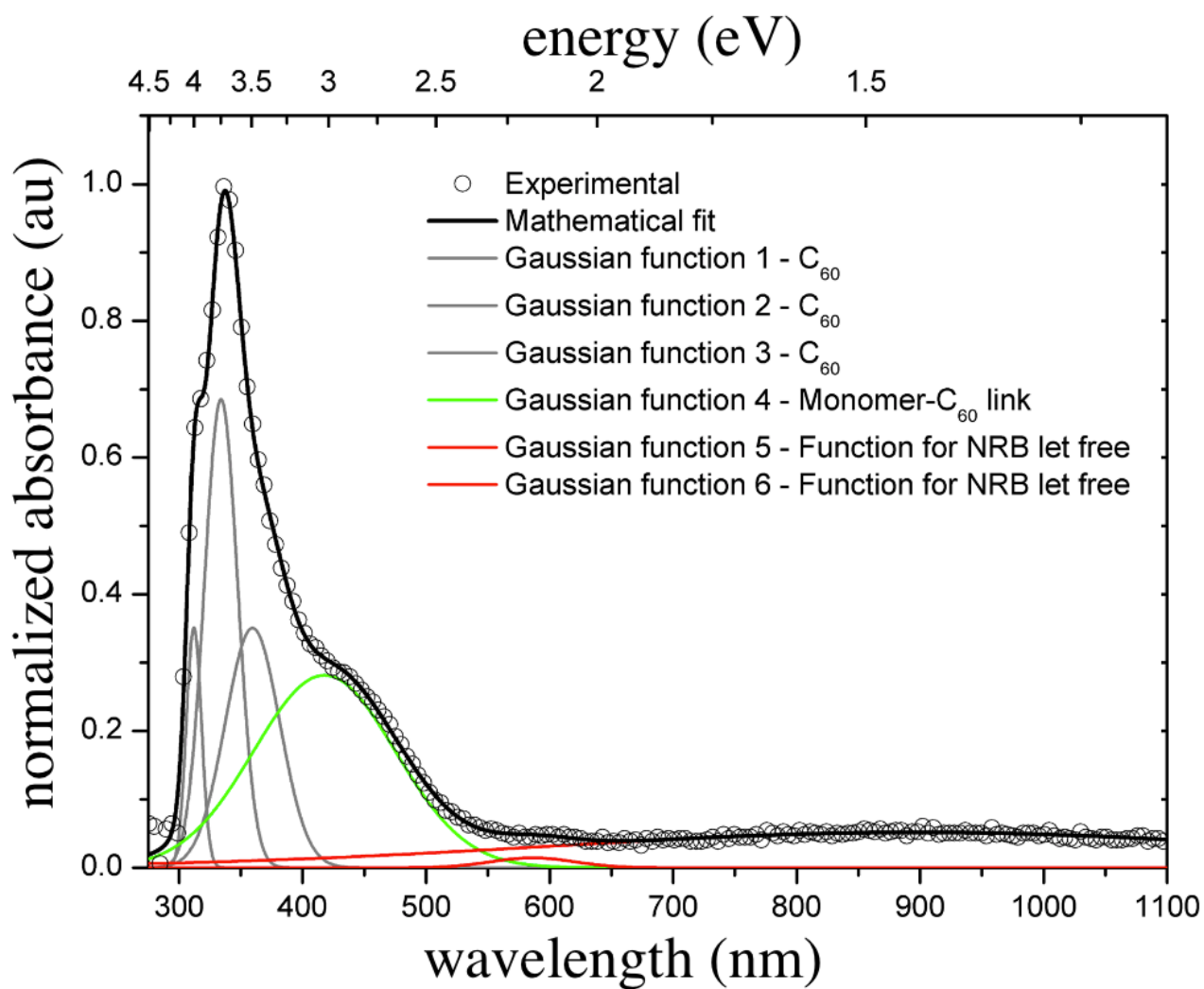


**Figure S3.** Gaussian fits of the UV-visible spectrum of a thin solid film of HSS-12.

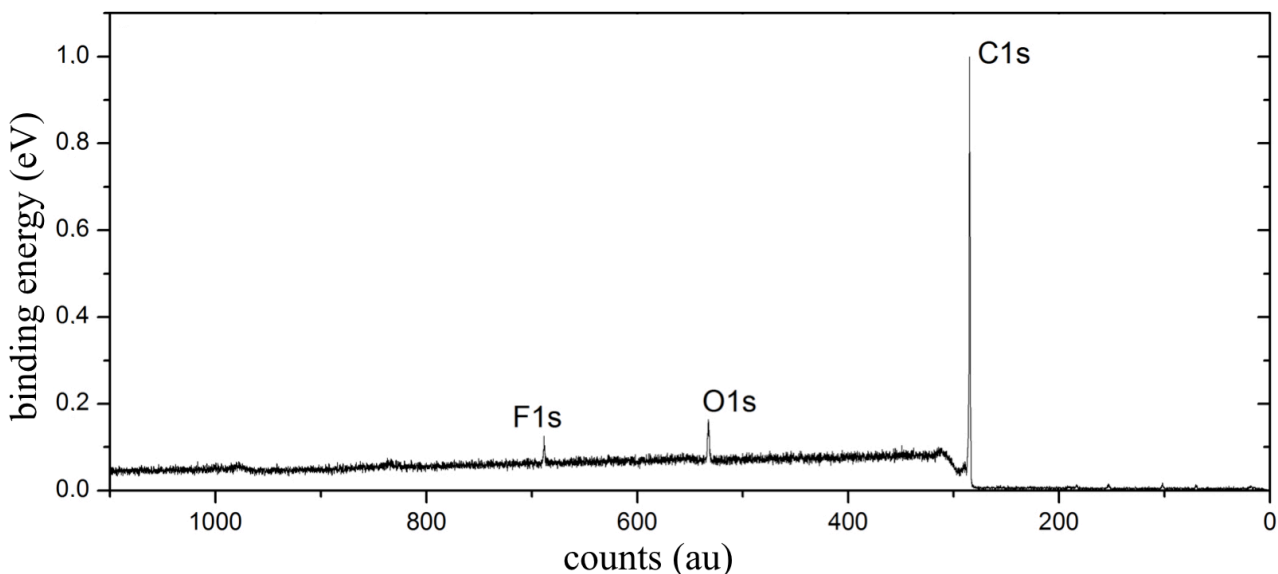


**Figure S4.** Overview XPS spectrum of HSS-12 deposited on to ITO/glass without heat treatment. Note the absence of indium and tin peaks indicating that the film is at least 10 nm thick. The F1s peak most likely arose from Teflon<sup>®</sup> filters used to filter solutions prior to deposition.

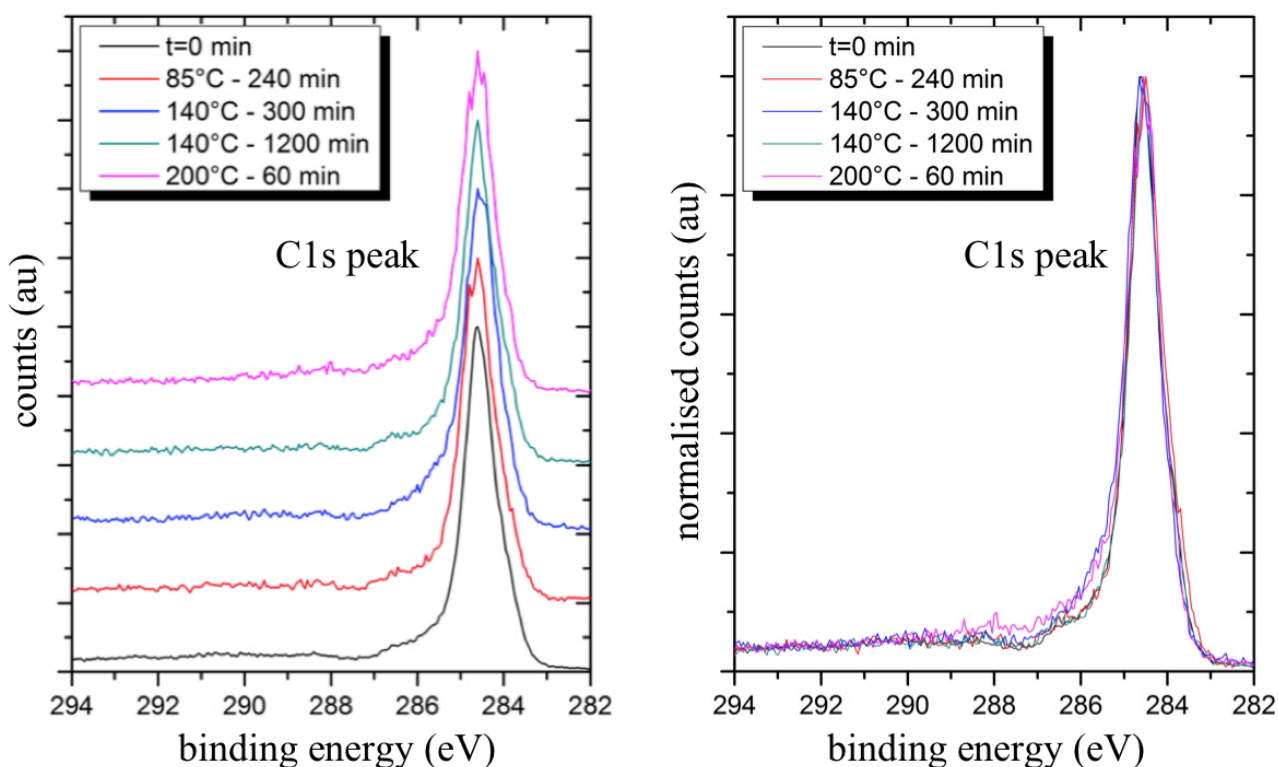


**Figure S5.** Carbon 1s XPS peaks from HSS-12 thin films on ITO/glass following various annealing treatments. In (a) the curves are stacked, and in (b) they are normalised and superimposed. It should be noted that we found that with increasing annealing times and temperature, the total quantity of F and O were found to decrease in the film, indicating that the F contaminant was volatile (probably polytetrafluoroethylene monomers) and also that some oxygen was adsorbed during the preparation of the polymers and their films.

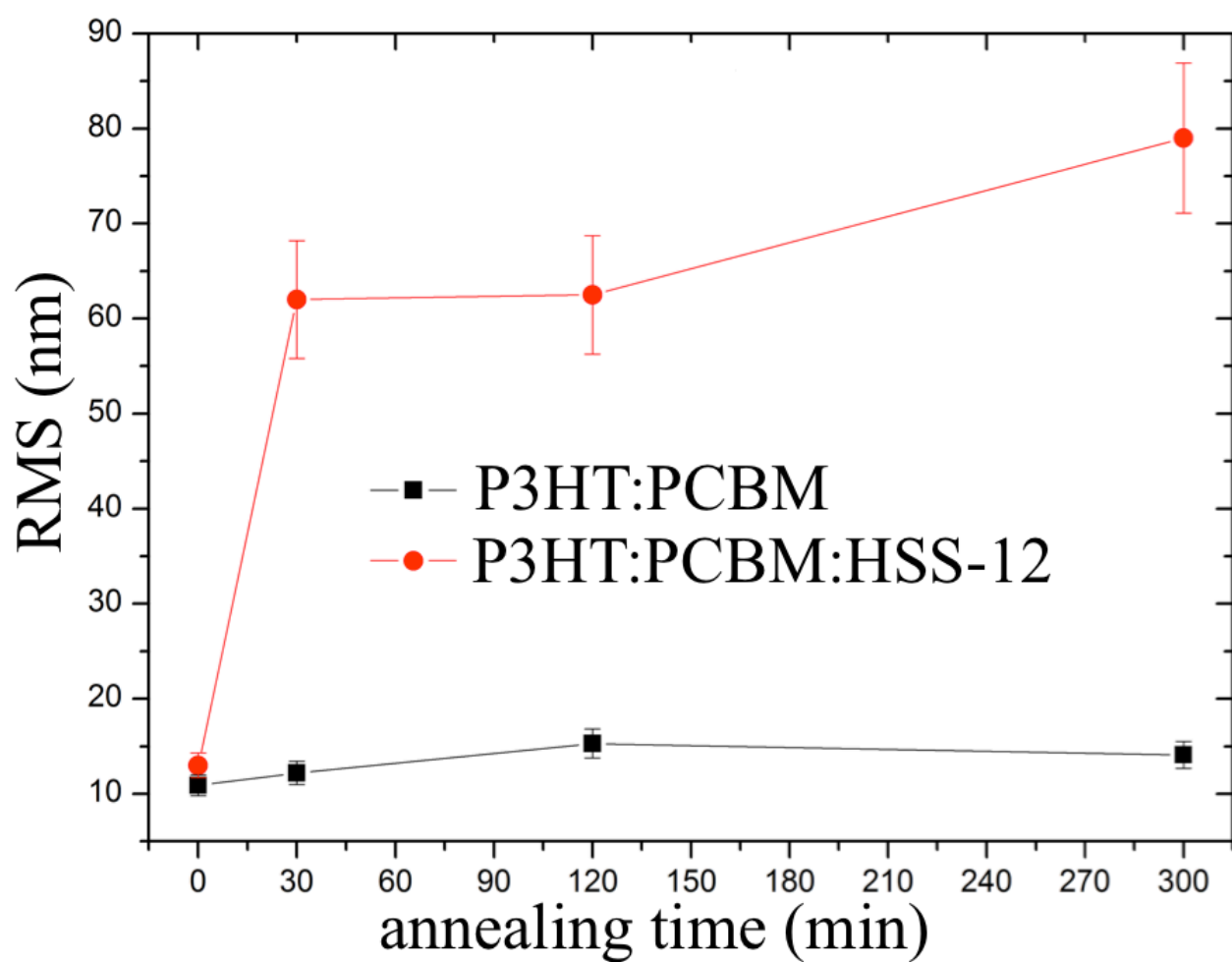


**Figure S6.** Evolution of surface roughness of P3HT:PCBM and P3HT:PCBM:HSS-12 with time. Annealing performed at 140 °C under nitrogen atmosphere.

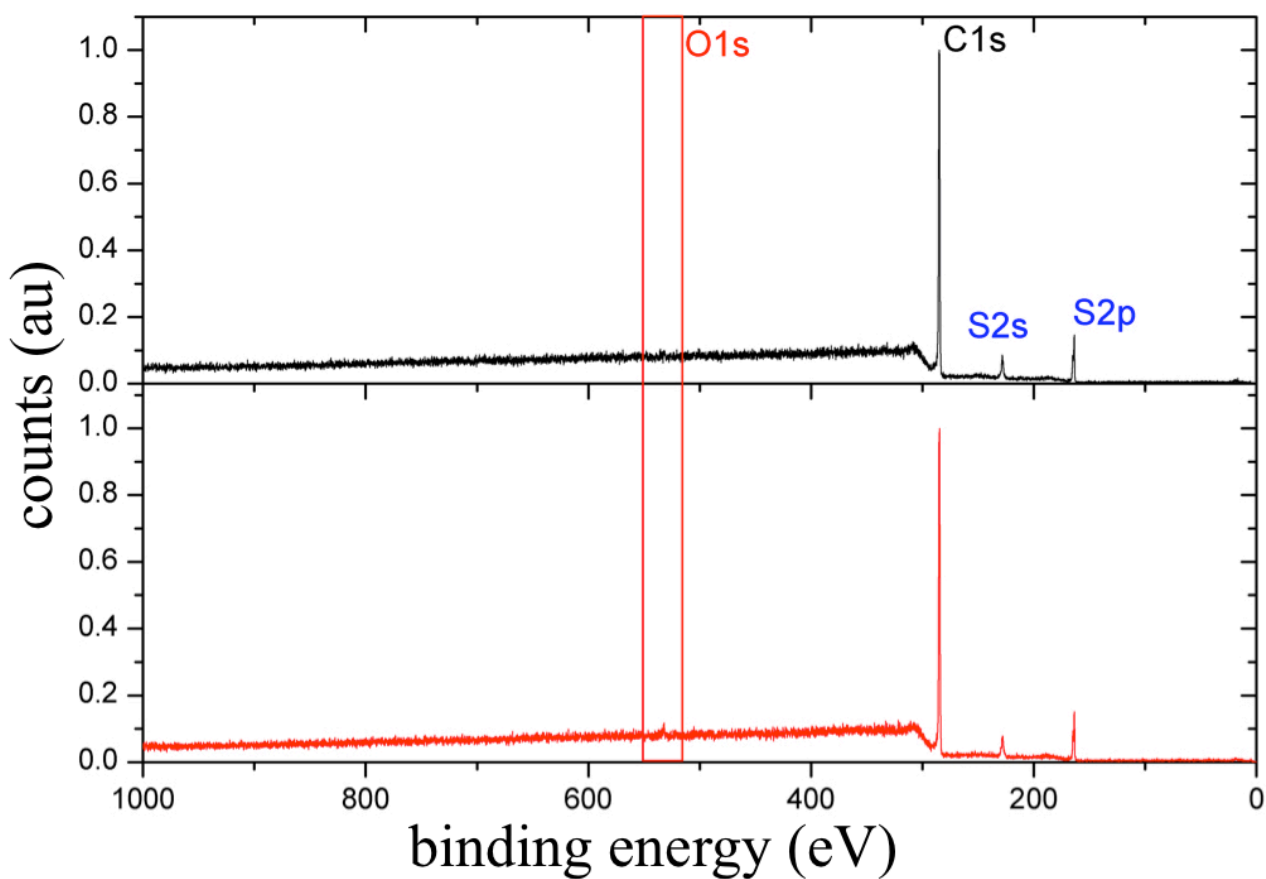


**Figure S7.** Overview XPS spectra for: (above) P3HT:PCBM; and (below) P3HT:PCBM:HSS-12 blends at  $t = 0$ .

**Table S1.** XPS in UHV indicated relative elementary concentrations with annealing in thin-film blends in nitrogen atmosphere. The sulfur concentration was calculated as an average over the cross-sections of S2s and S2p signals, resulting in similar compositions.

Annealing time (min)	P3HT:PCBM			P3HT:PCBM:HSS-12		
	C	S	O	C	S	O
0	100	9.6	0	100	7.9	0
120	100	6.5	0.7	100	8.1	1.7
300	100	6.7	1.8	100	7.8	1.0

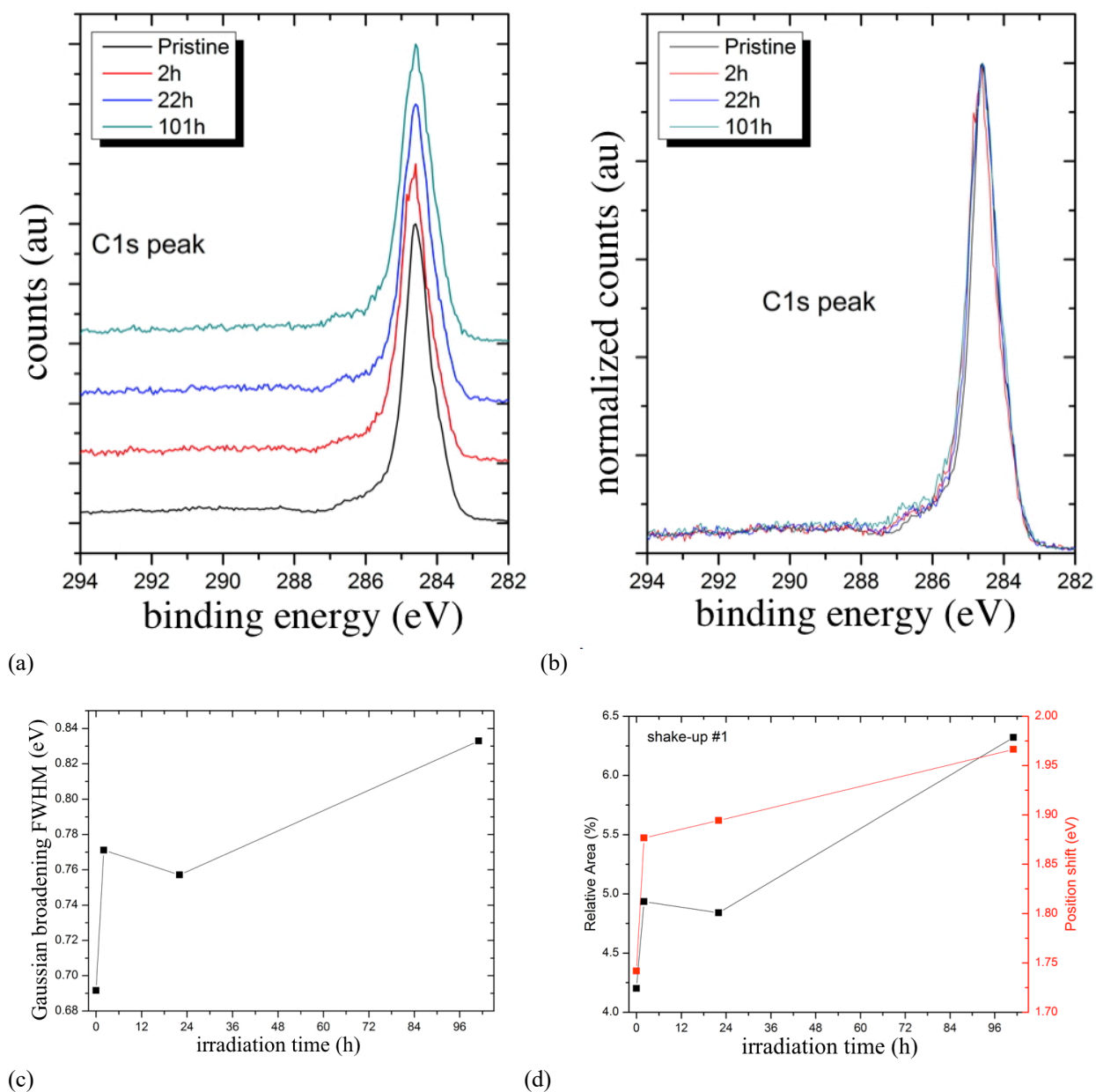
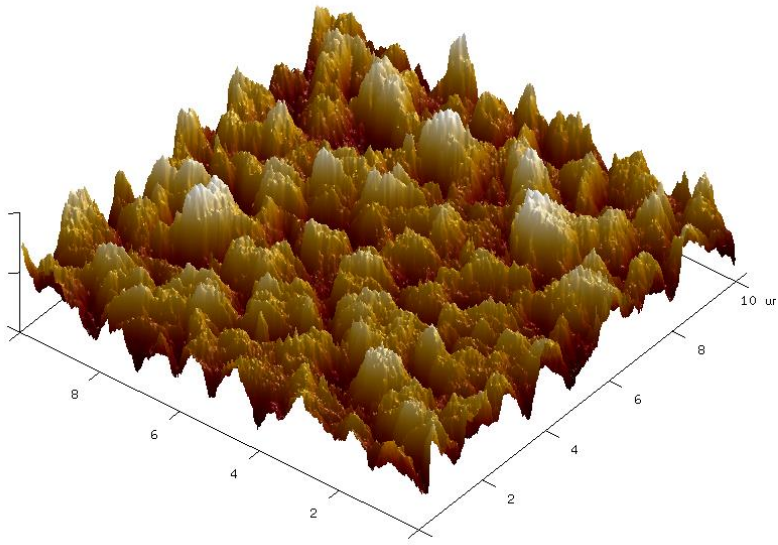
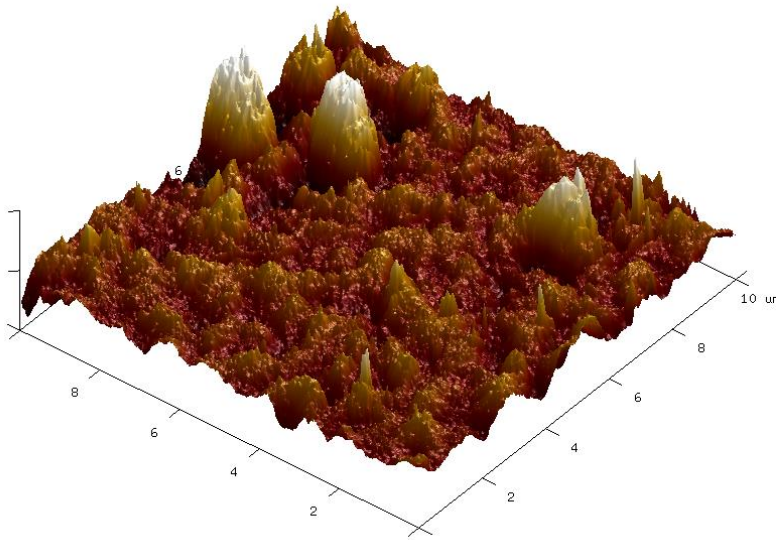


**Figure S8.** C1s core level spectra of HSS-12 as a function of the irradiation time. All films were on ITO/glass. In (a), the spectra are stacked. In (b), they are normalized and superimposed. Only slight changes of the position and intensity of features at higher binding energies compared to the main line are visible ( $> 285$  eV), which might be due to a change of the shake-up position and area or additional oxidized C species.



(a)

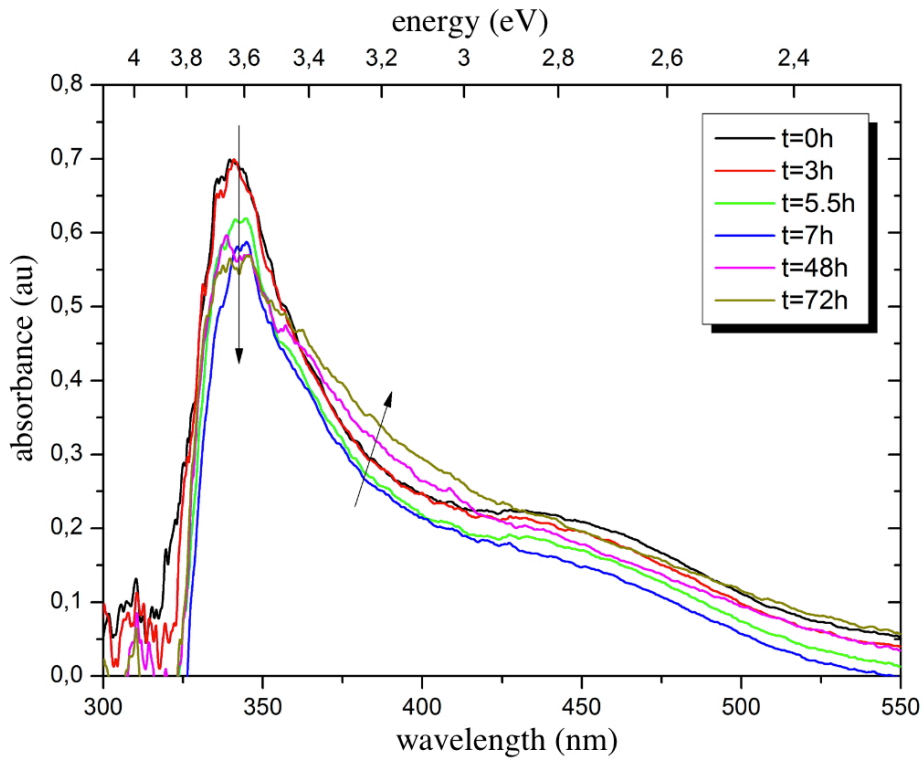


(b)

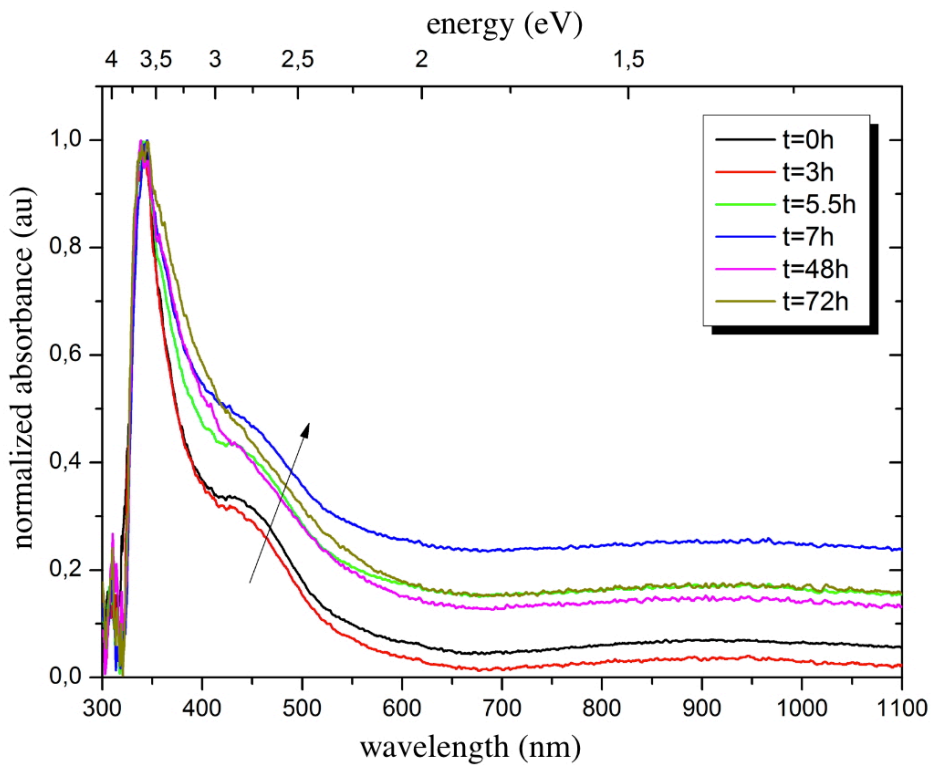
**Figure S9.** 3D AFM reconstructions of (a) P3HT:PCBM and (b) P3HT:PCBM:HSS-12 nanomorphologies illuminated under AM1.5 conditions and nitrogen atmosphere for 120 h. The images cover 10 x 10  $\mu\text{m}$  areas.

**Table S2.** XPS indicated relative atomic concentrations in thin-film blends before and after treatment with light under AM1.5 conditions and N<sub>2</sub>. The sulfur concentration was calculated from an average of S2s and S2p signals.

<b>Annealing time</b> <b>(min)</b>	<b>P3HT:PCBM</b>			<b>P3HT:PCBM:HSS-12</b>		
	<b>C</b>	<b>S</b>	<b>O</b>	<b>C</b>	<b>S</b>	<b>O</b>
<b>0</b>	100	9.6	0	100	7.9	0
<b>96</b>	100	7.7	0.7	100	7.9	1.6

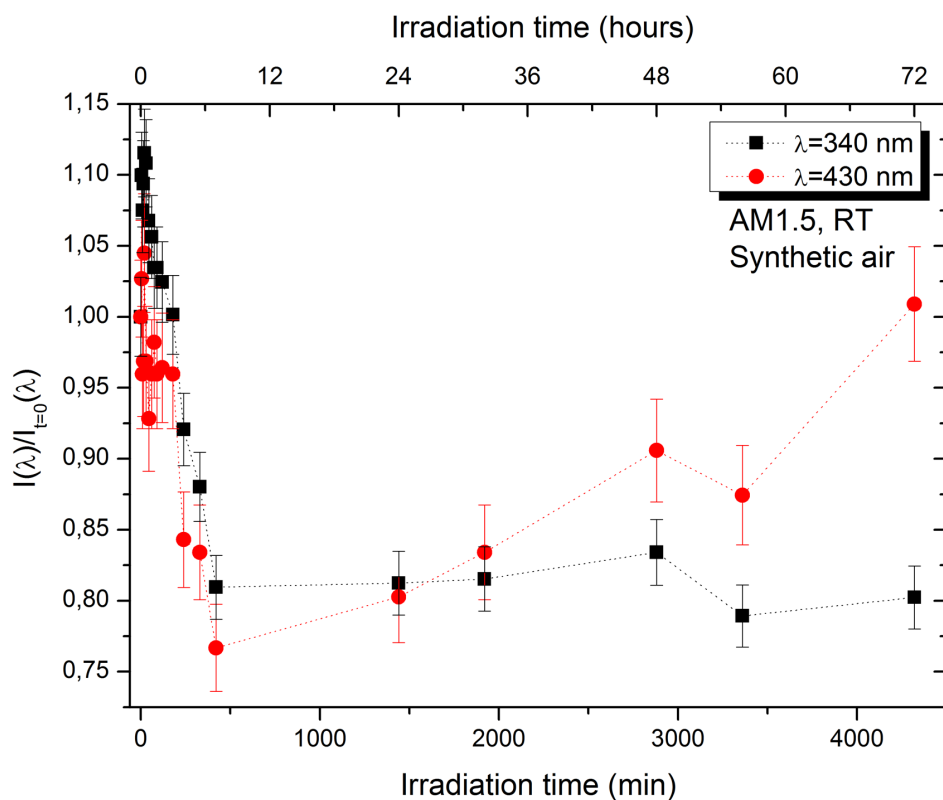


(a)

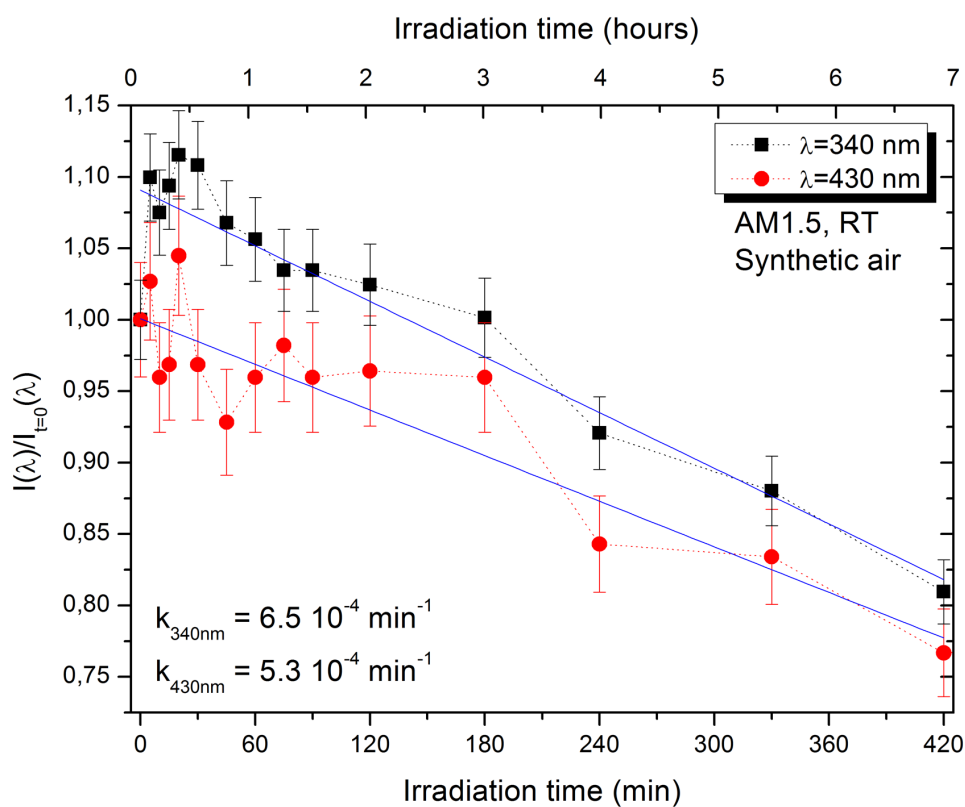


(b)

**Figure S10.** Evolution of UV-visible spectra under AM1.5 conditions and synthetic air. While in (a), no normalisation was applied, in (b) normalization was used to clarify the effect.



(a)



(b)

**Figure S11.** Evolution of UV-visible spectra under photo-oxidation conditions with respect to the pristine sample. (b) shows a zoom of the region below 7 h with a tentative linear fit of each curve with the associate rate constants.

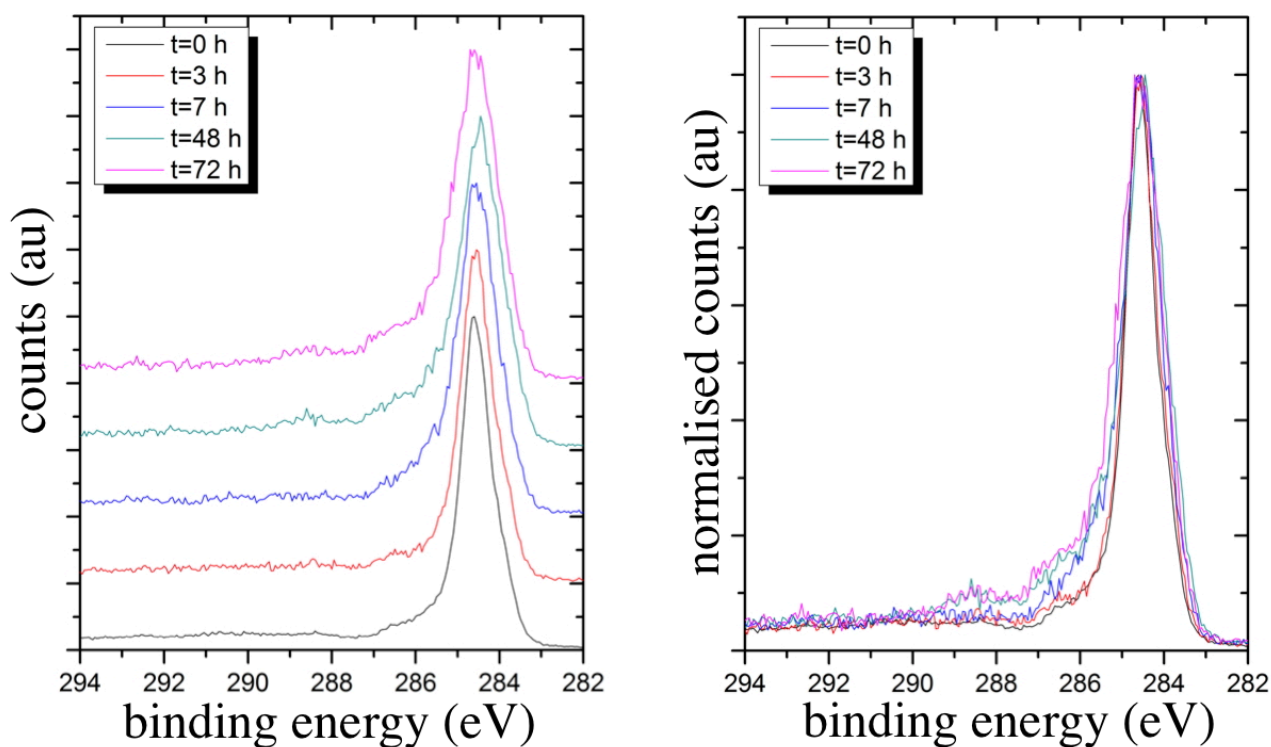


**Figure S12.** Carbon 1s XPS peak for HSS-12 polymer (thin film on ITO/glass substrate) submitted under irradiation times under synthetic air atmosphere. In (a), the spectra are stacked and in (b) they are normalized and superimposed.

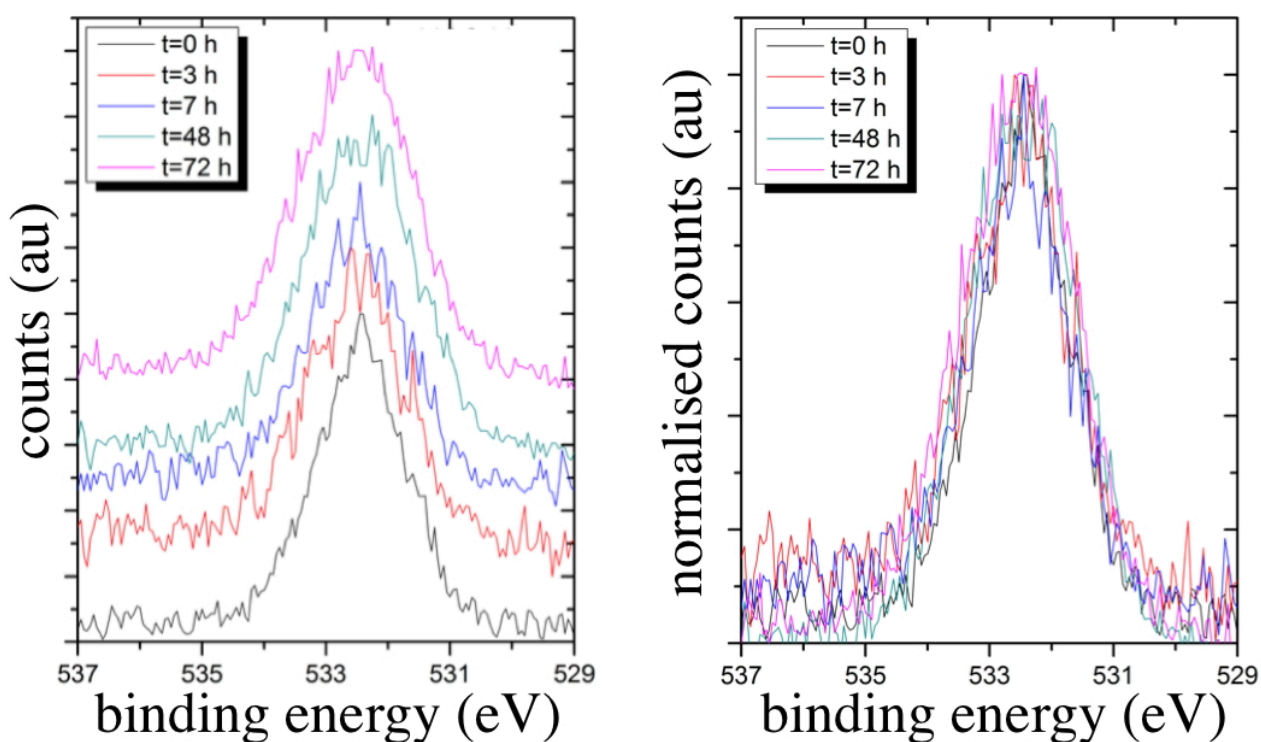


**Figure S13.** Oxygen 1s XPS spectra for HSS-12 polymer (thin film on ITO/glass substrate) submitted under irradiation times under synthetic air atmosphere. In (a), the spectra are stacked and in (b) they are normalized and superimposed.

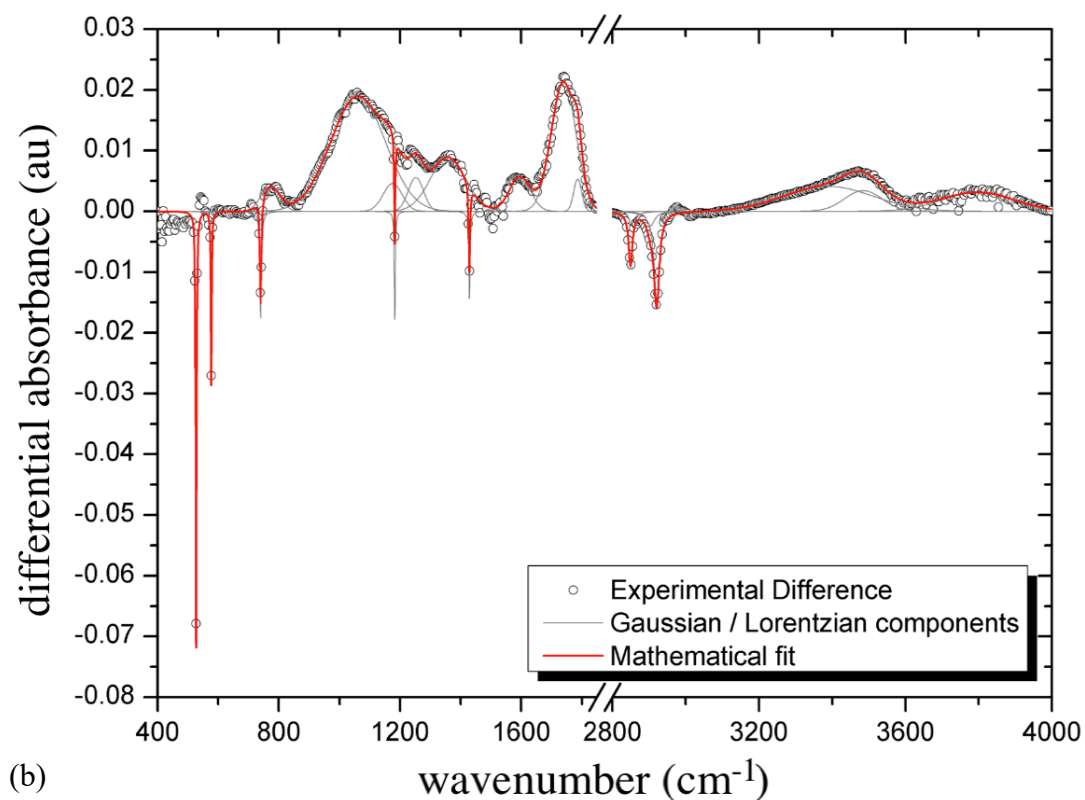
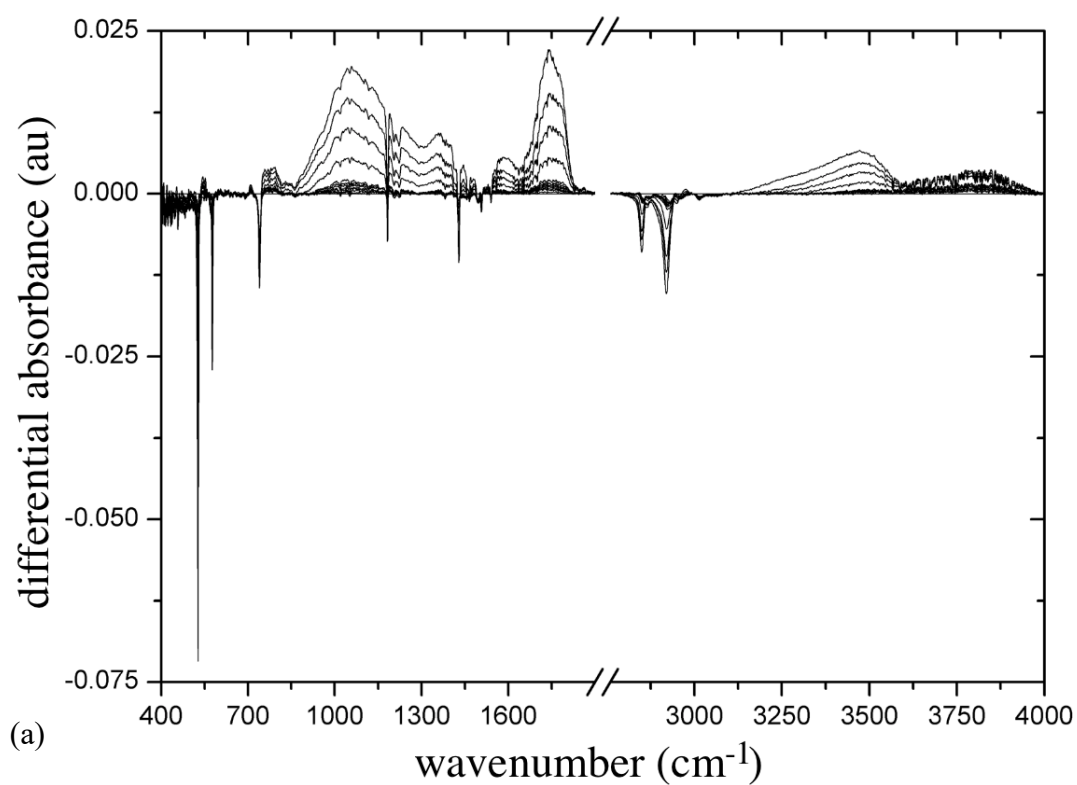
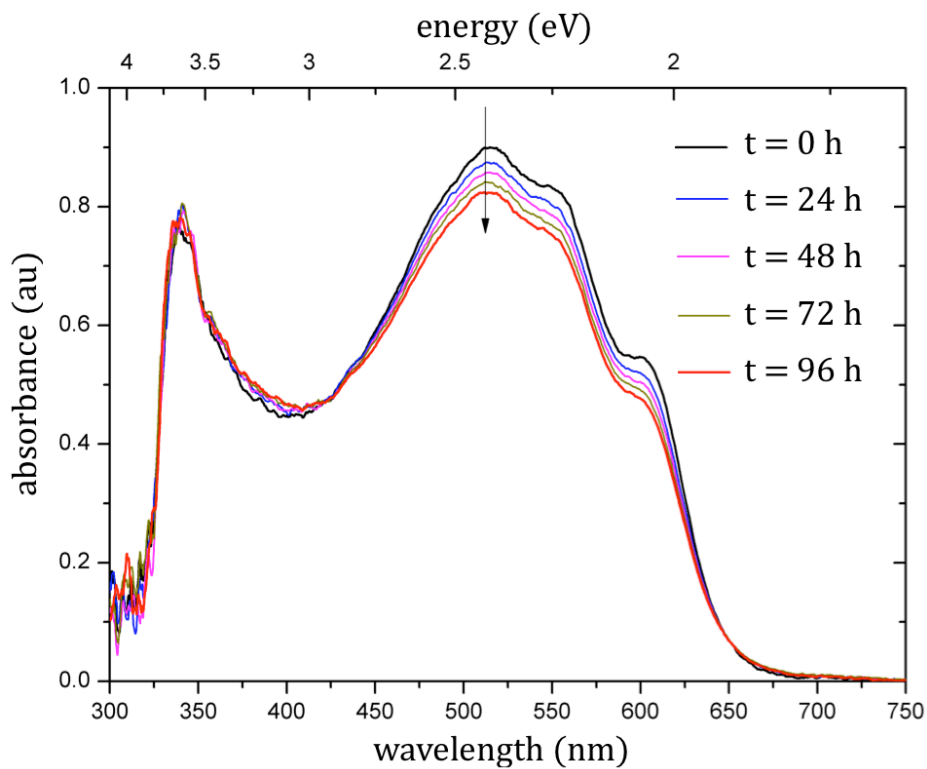
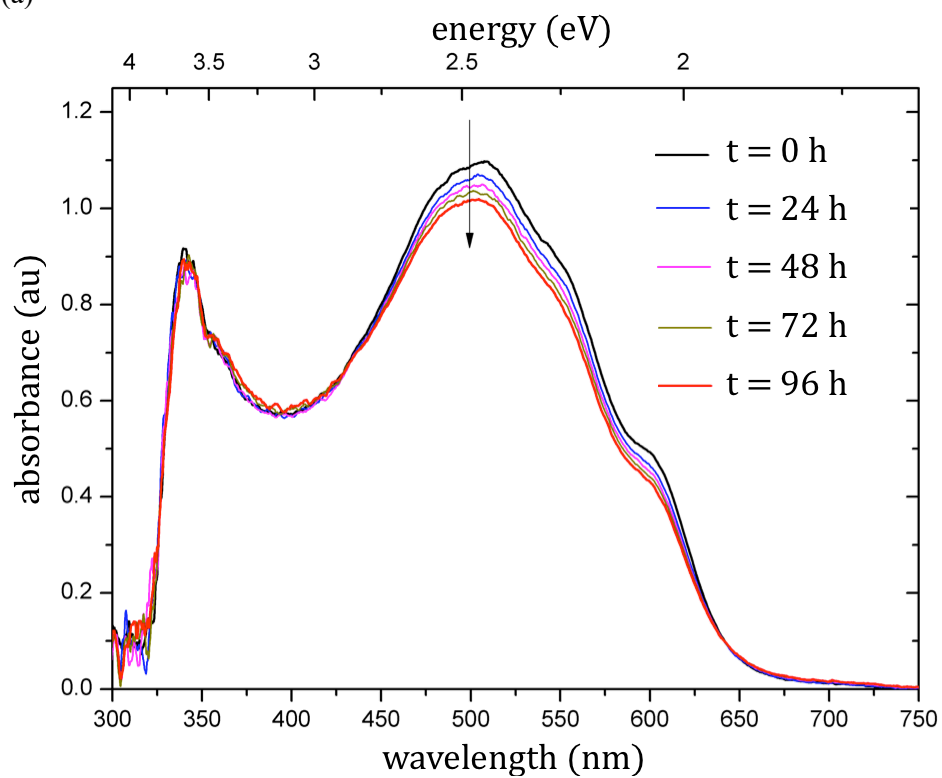


**Figure S14.** Evolution in time of HSS-12 FTIR spectra during photo-oxidation. In (a), one can find the superposed spectra during degradation and in (b) the mathematical fit for  $t=96$  h is presented. The time steps for (a) is the same as used in Figures S10.



(a)



(b)

**Figure S15.** Evolution with photo-oxidation of the UV-visible spectra of: (a) P3HT:PCBM; and (b) P3HT:PCBM:HSS-12.

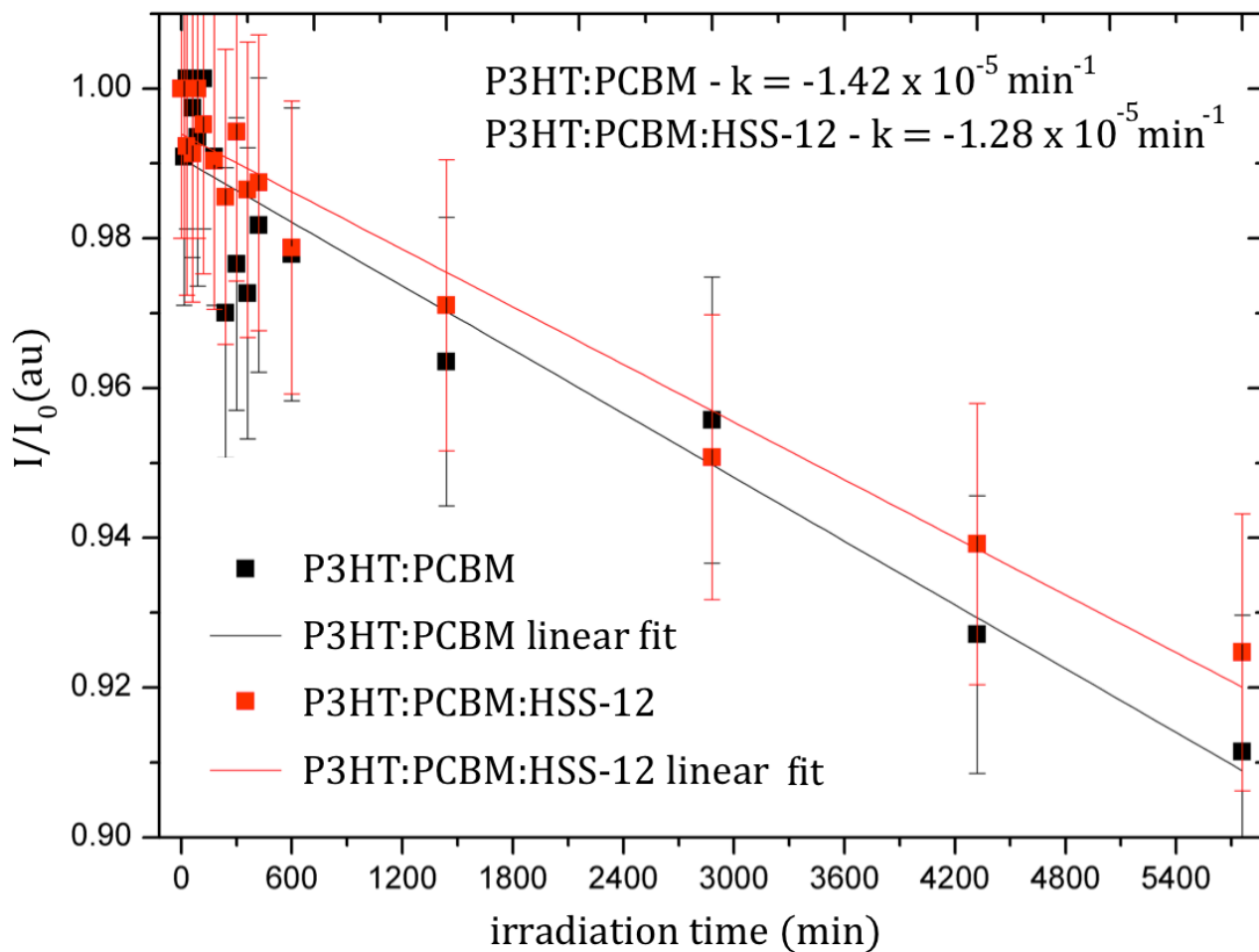


**Figure S16.** Evolution with time of the UV-visible spectra of P3HT:PCBM and P3HT:PCBM:HSS-12 undergoing photo-oxidation.

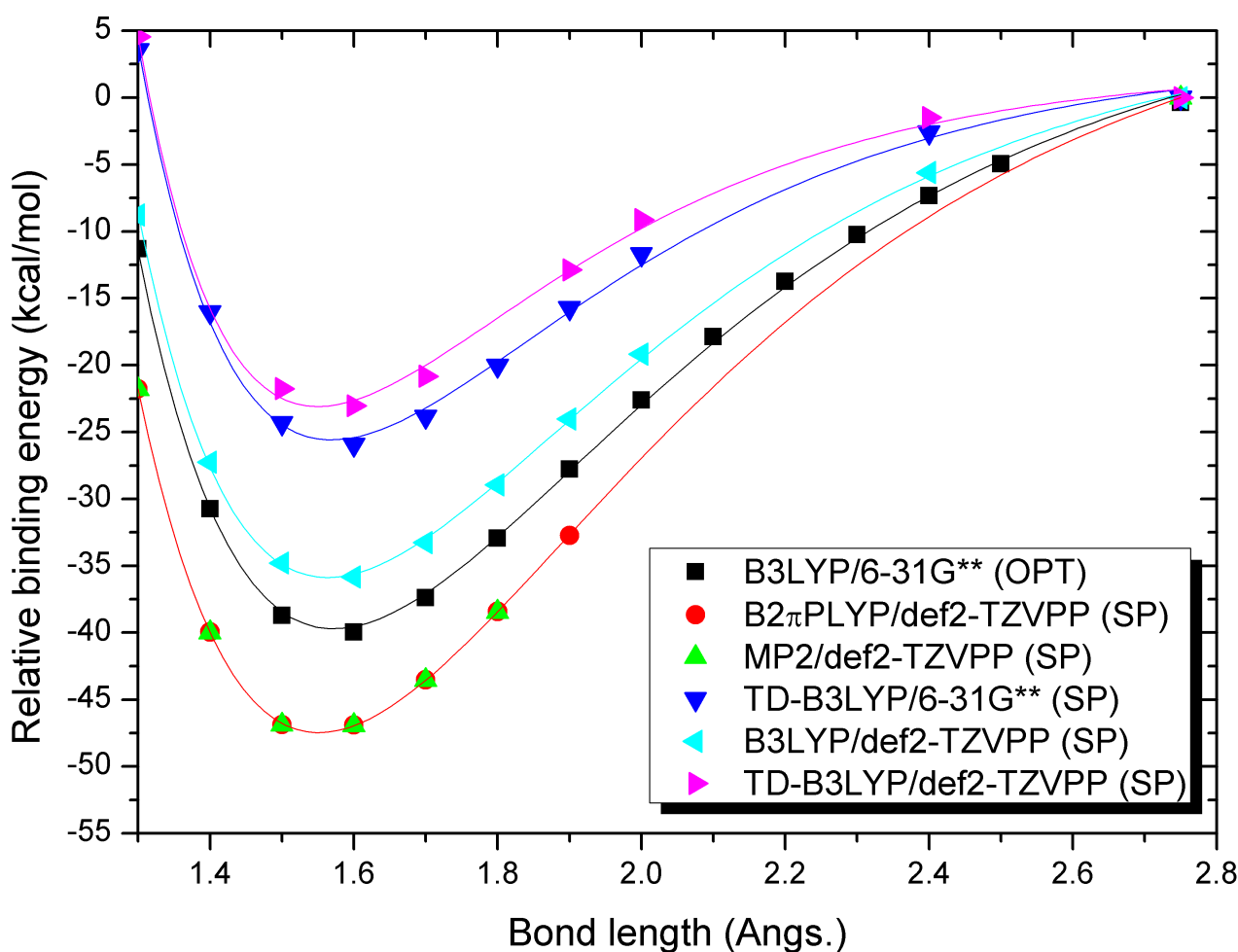


**Figure S17.** Bond-dissociation reaction coordinate scan for the ATRAP proposed model material calculated by different level of theories, under fully optimization (OPT) or single-point energy evaluations (SP). They were also calculated on the first excited state (TD label) showing that this bond tends to be photochemically cleaved with moderate energies (20 to 50 kcal mol<sup>-1</sup>).

Note: the theoretical methodologies used for this calculation cover the specific needs of the system, in terms of basis set and level of theory. Both electronic density and wave-function based methods have been used to test if this result might have a methodology-dependent behaviour.

To make sure that this was not a coincidence concerning a high radical stabilization by the monomer molecule, we also studied the two other configurations shown in Figure S18, where both result from the same attacking route on the fullerene.

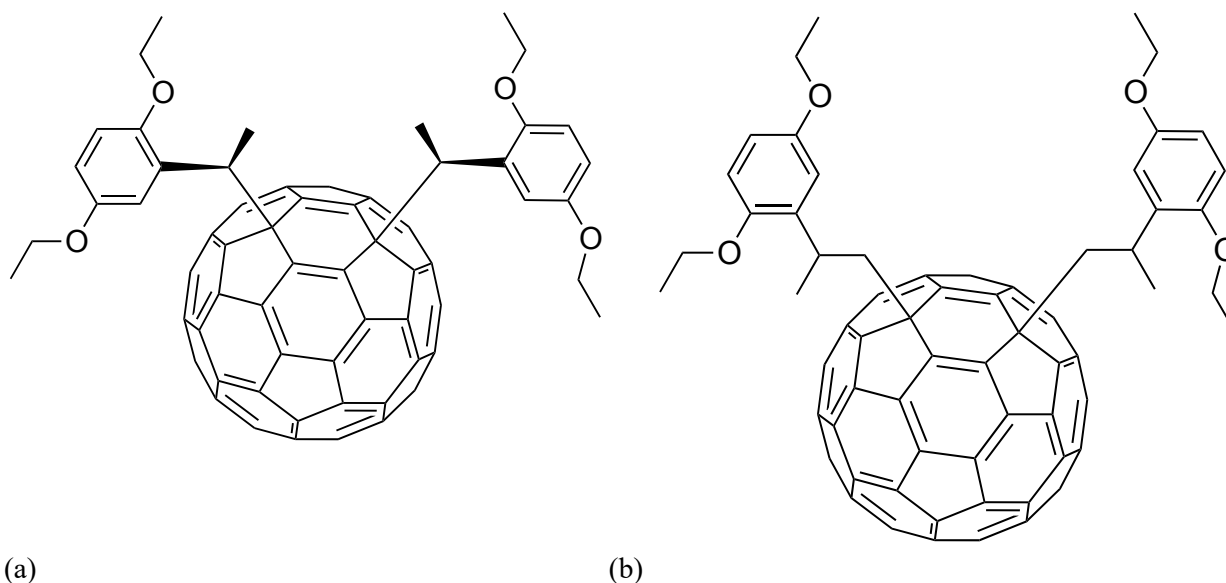
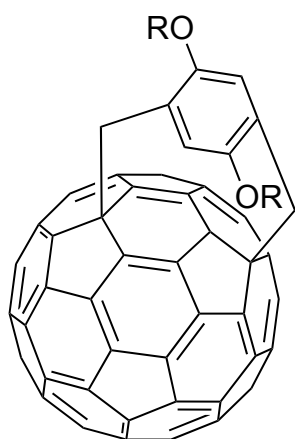


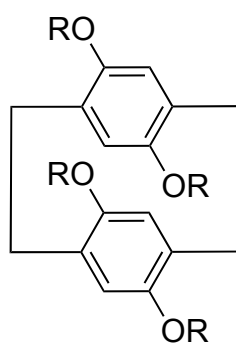
**Figure S18.** Modified ATRAP structures used to study the influence of the  $-\text{CH}_2-$  link on stabilities.

Note: in (a), one hydrogen atom from the  $-\text{CH}_2-$  linking group has been replaced by a methyl and in (b), one tertiary carbon atom has been added between the  $-\text{CH}_2-$  and the comonomer. For the former, bond dissociation energies were found to be of the order of  $\sim 48 \text{ kcal mol}^{-1}$  and, for the latter of the order of  $\sim 35 \text{ kcal mol}^{-1}$ , within the B3LYP/6-31G\*\* level of theory. This corroborates the common-sense that tertiary carbons stabilize radicals, leading, in this case, to more unstable monomer-fullerene link. Please note that Normally, C-C single bonds have a bond dissociation energy comprised between  $90$  and  $100 \text{ kcal mol}^{-1}$ . Moreover, one should keep in mind that, at room temperature ( $25 \text{ }^\circ\text{C}$ ), the available thermal energy is  $0.593 \text{ kcal mol}^{-1}$ .

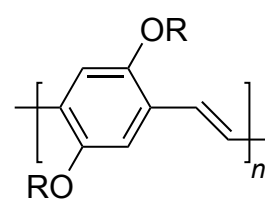
The BDE value of  $55 \text{ kcal mol}^{-1}$  comes from a triple- $\zeta$  calculation instead of a double- $\zeta$  one. This does not disagree with the results presented just above. The difference here is found on the fact that we now used a bis-attacked fullerene model with terminal bromine atoms on the comonomer, using the 6-311G\*\* basis set. As it was not possible to calculate this reaction using periodic boundary conditions, we assumed, for the sake of simplicity, that the depolymerization process starts at chain ends. Empirically we expect that for middle-chain bonds, these energies should be even lower due to the fact that both  $-\text{CH}_2-$  groups are free to form vinylic bonds with the cycle, whereas for the case where we have a bromine terminal atom, this cannot be the case.



(a)



(b)



(c)

**Figure S19.** Three possible products of degradation resulting from the formation *p*-quinodimethane during the thermal treatment of PFBMBs, resulting from thermal treatment: (a) bridged fullerene resulting from free radical attack of the *p*-quinodimethane on C<sub>60</sub>; (b) a [2,2]-1,4-cyclophane derivative; and (c) oligo(phenylene vinylene).

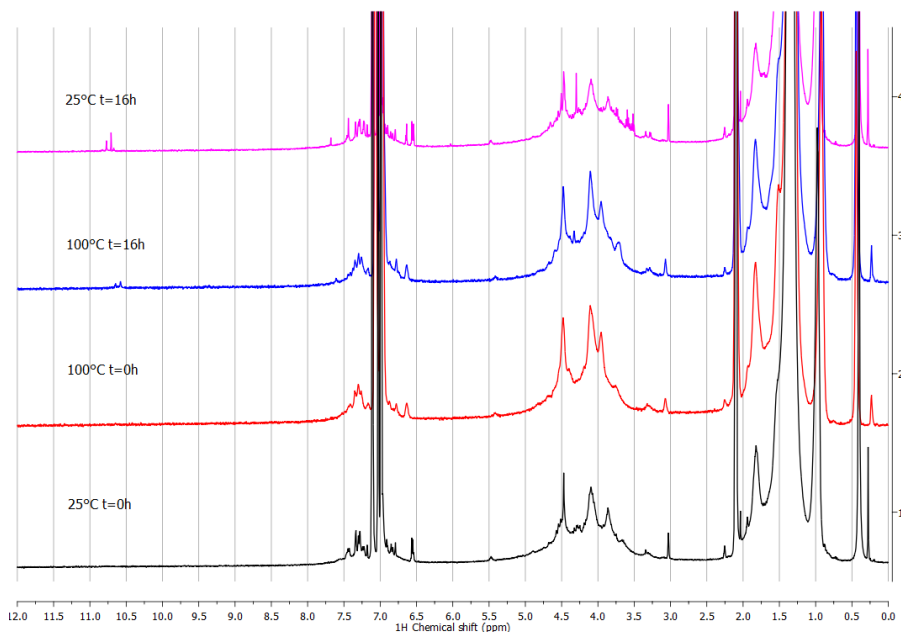


**Figure S20.**  $^1\text{H}$ -NMR spectra of HSS-12 in  $d_8$ -toluene solution heated to 100 °C for 16 h in a nitrogen-sealed glass tube. The first spectrum was acquired at  $t=0$  at 25 °C, with subsequent spectra obtained every 5 min up to 16 h. The final spectrum was recorded at 25 °C but after 16 h at 100 °C.

Note: The residual peaks of toluene in  $d_8$ -toluene are found at 2.08, 6.97, 7.01 and 7.09 ppm. The peaks found at 0.43 and 3.03 ppm correspond to water and methanol, respectively.

On heating, a broadening of the peaks both in the aromatic region as well as in the 3.5-5.0 ppm region occurs, which is associated to the region where the  $-\text{CH}_2-$  peaks of the monomer-fullerene link are found along with triplets arising from protons alpha to ether groups.

From 2 h of heating on, a peak located at 4.3 ppm appears and its intensity increase with time, being maximum when the sample is cooled down again back to 25 °C. Furthermore, a multitude of new peaks can be found in the region around 3.6 ppm. This is more clearly seen in Figure S21 below.

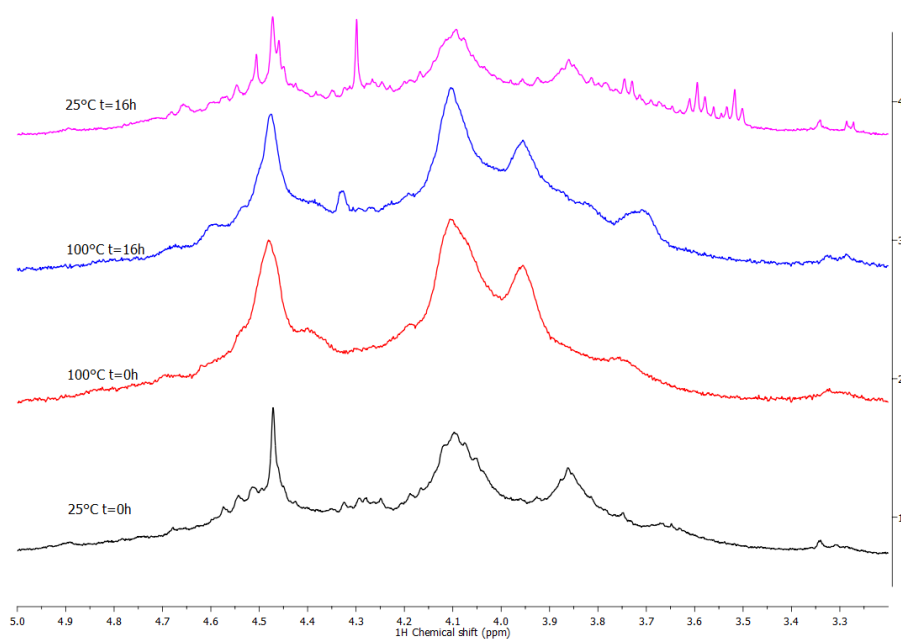


**Figure S21.** <sup>1</sup>H-NMR spectra of HSS-12 *d*<sub>8</sub>-toluene solution heated to 100 °C for 16 h - zoom in the 3.5-5.0 ppm regions.

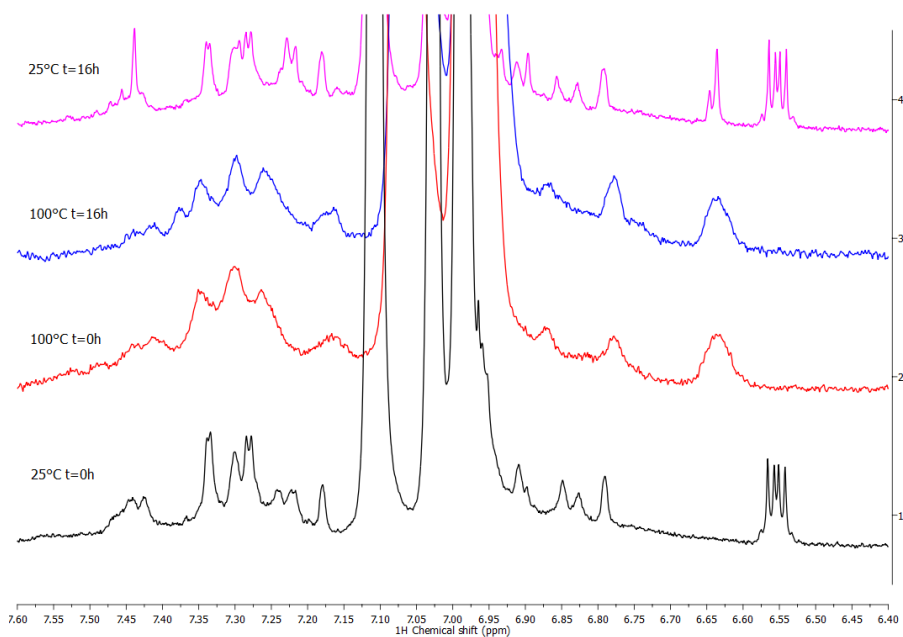


**Figure S22.**  $^1\text{H}$ -NMR spectra of HSS-12  $d_8$ -toluene solution heated to 100 °C for 16 h - zoom in the aromatic regions.

Notes: The broad peaks at 7.25 and 7.45 ppm at the beginning of the experiment broaden during heating and then on cooling, gives rise to better defined peaks.

Also, the multiplets centred at 6.55 ppm are hindered during heating and are once again detectable when the sample is cooled back down to room temperature. Since the beginning of the heating process, a broad peak centred at 6.55 ppm appears and upon cooling is finally resolved as doublet or a set of two singlets found closely together.

## References

1. R. Hesse, T. Chassé, P. Streubel and R. Szargan, *Surf. Interface Anal.*, 2004, 36, 1373.
2. J.J. Yeh and I. Lindau, *Atom. Data Nucl. Data Tables*, **1985**, 32, 1.